Phase noise measurements and diagnoses of a large array of fiber lasers by PISTIL

Bastien Rouzé, Ihsan Fsaifes, Severine Bellanger, Matthieu Veinhard, Thomas Rousseaux, Jérome Primot, Jean-Christophe Chanteloup, Cindy Bellanger

Phase noise measurements and diagnoses of a large array of fiber lasers by PISTIL

BASTIEN ROUZÉ,[1,*] IHSAN FSAIFES,[2] SEVERINE BELLANGER,[2] MATTHIEU VEINHARD,[2] THOMAS ROUSSEAUX,[1] JÉROME PRIMOT,[1] JEAN-CHRISTOPHE CHANTELOUP,[2] AND CINDY BELLANGER[1]

[1] *DOTA, ONERA, Université Paris Saclay –91120 Palaiseau, France*
[2]*LULI, CNRS, Ecole Polytechnique, CEA, Sorbonne Université, Institut Polytechnique de Paris–91120 Palaiseau, France*
*bastien.rouze@onera.fr

Abstract: One of the most promising solutions to access high power laser chains is to achieve a coherent combination of a large number of elementary lasers. To interfere constructively, these laser sources should be identical and operate under the same conditions. However, despite these efforts, differential delays appear in the course of time, which must be compensated for. While designing the required correction system, knowing the behavior of a laser as a function of the environmental conditions is not crucial, whereas having access to the differences in the behaviors of identical lasers is, leading to difficulties in modelling. The purpose of this paper is to illustrate how a large set of lasers can be simultaneously analyzed to estimate their variations and optimize a correction system. The XCAN laser relies on 61 fiber amplifiers, which are as identical as possible. This state of the art femtosecond digital laser therefore appears as an ideal candidate to study a large number of fiber lasers working under controlled conditions.

1. Introduction

Coherent Beam Combining (CBC) of fiber amplifiers is today in the industrialization process [1-3]. Proposed as a method to increase both peak and average powers of a laser beam [4, 5], it has undergone important developments in the last fifteen years, allowing more and more combined channels while scaling the peak and average powers with excellent beam quality under various operating regimes [6-11].

The main objective of CBC is to make N beams interfere constructively in the far-field, which requires the phase of each beam being controlled and set equal altogether via a servo-loop [10-14]. Applying such an algorithm will minimize the piston phase difference between two or more beams relatively to a reference beam or a reference value. Several laser architectures have been proposed in the last 20 years, the most common ones being the superposition of the beams in near-field or filled-aperture [6] and the optical phased array (OPA) arrangement or tiled-aperture [7]. The latter also has the advantage of controlling the segmented wavefront, made up of all the phases of the N beams, in order to perform far-field beam shaping [15].

These new laser systems call for the use of a very large number of identical systems, such as the fiber amplifiers or the opto-mechanical parts, in order to design the most identical N elementary channels possible. As a consequence of their forthcoming industrialization, the designers-suppliers of fiber lasers and amplifiers must conceive almost identical elementary bricks, or their assembly in an optical head, according to the specifications provided by CBC engineers (power range, noise, etc.). To our knowledge, there is no self-referenced collective

measurement mean, independent of the far field or near field phasing loop, for diagnoses of such fiber laser arrays.

In this paper, we propose investigating the phase noise properties of numerous a priori identical laser channels functioning altogether by performing a collective phase measurement of the laser beams by the use of a PISton and TILt interferometric sensor (PISTIL), a reference-free segmented wavefront analyzer which fits with the segmented pupil architecture [10,17-21]. We then exploit the measurements to highlight identical behaviors or differences in the fiber laser array. The experiment is conducted from the XCAN laser (X-Coherent Amplified Network, X is a short for École Polytechnique), a CBC-class laser system combining up to 61 fiber amplifiers arranged in a hexagonal mesh [7, 16], which has recently demonstrated state of the art performances [15]. The XCAN and PISTIL setups are described in section 2, and the measurement operation in section 3. We perform open-loop measurements on the XCAN laser (without enabling CBC); in order to present in section 4 multiple characterizations of the phase noise of the laser channels.

2. XCAN and PISTIL description

The XCAN laser [7, 15, 16] relies on tiled-aperture CBC configuration where 61 Yb-fiber amplified beams are stacked side by side in a planar hexagonal array arrangement (Figure 1). The beams are collimated using a high fill factor hexagonal microlens array. Their central wavelength is $\lambda = 1032$ nm. The phase of each individual beam is controlled in the kHz regime through the combined use of Variable Optical Delay Lines (VODL: ±3 cm range and 0.1 µm increment) and piezo-mechanical Fiber Stretchers (FS: with a dynamic range of ±19 µm, corresponding to phase shifts of ±18.4 λ). They are stacked in Delay & Phase Adjustment Modules (DPAM). The closed-loop phase stabilization is performed using a collective interferometric measurement method through active phase control [12, 22] and a Stochastic Parallel Gradient Descent algorithm [13], with a residual phase below $\lambda/50$ RMS, measured from two fibers interference [7]. The CBC is achieved when focusing the 61 collimated beam pupil with a single lens. This architecture demonstrates high agility as the near field amplitude and phase are controlled in real time permitting far-field beam shaping [15]. In this paper, XCAN laser is only operated in open-loop mode, i.e. without any active phase correction.

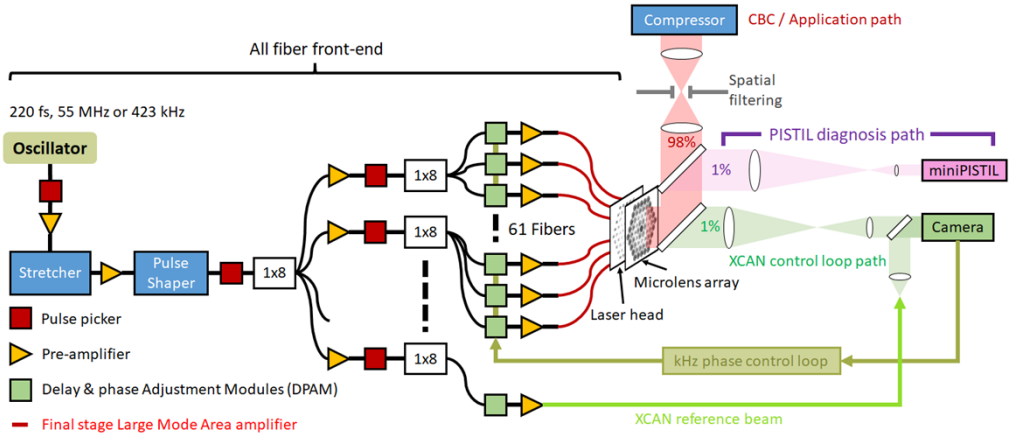

Figure 1: The XCAN laser setup using up to 61 amplified laser fibers. Science application laser path is drawn red (98%). The phase control path (olive/green) is not switched-on in the scope of this open-loop diagnosis. The miniPISTIL transportable prototype (purple, 1%) is implemented using a reduced XCAN segmented pupil image.

The PISTIL (PISton and TILt) interferometer is a concept of self-referenced lateral shearing interferometer [17]. It has been designed for fine sensing of phase piston and tip/tilt of a segmented wavefront, either relative to an absolute reference surface (or a laser beam), or

relative to an arbitrary reference value in time. It combines the use of a holes mask, a diffraction grating and a detector to make neighboring beams interfere in near field. This interferometric figure, called "pistilogram", contains several 2-wave interference patterns whose distribution depends on the geometry of the laser pupil. A magnifying telescope can be used to adapt the mask size to the camera. A Fourier Transform based algorithm is applied to the fringes to obtain the phase difference between each laser beam. Then, a generalized matrix inversion is being computed for the phase of each channel to be estimated from these differences [18, 20]. Such a process has proven to be noise resilient. Indeed, measurements taken out from previous researches show an accuracy in the hundredth of wavelength range ($< \lambda/100$) for static segmented wavefront sensing [19, 20], and a precision $< \lambda/200$ RMS (root mean square) allowing it to perform a channel-to-channel phase diagnosis below λ/20 RMS for closed-loop CBC systems [10, 21].

The PISTIL interferometer used in this work is a transportable prototype called "miniPISTIL" that can be quickly integrated on any type of laser array bench. Its 4-rings hexagonal holes mask has a 606 µm pitch and hole diameter of 300 µm. The diffractive optical element is a phase grating with a period of 97 µm. The camera is a JAI SP-5000 CXP4 of 2580 by 2048 pixels, and a pitch of 5 µm. A windowed mode of 448 by 448 pixels is made to allow fps boost up to 1000 Hz. To match the size of the pistilogram in relation of the holes mask, the telescope magnification is set to x0.4, with respect to an adequate sampling of the fringes (3 pixels per fringes).

The system is fed with a sample of the 61 collimated beams near field pupil (1% of power) imaged onto the interferometer (Figure 1, Figure 2a). When the full fiber laser array is active, the complete pistilogram obtained is shown in Figure 2b.

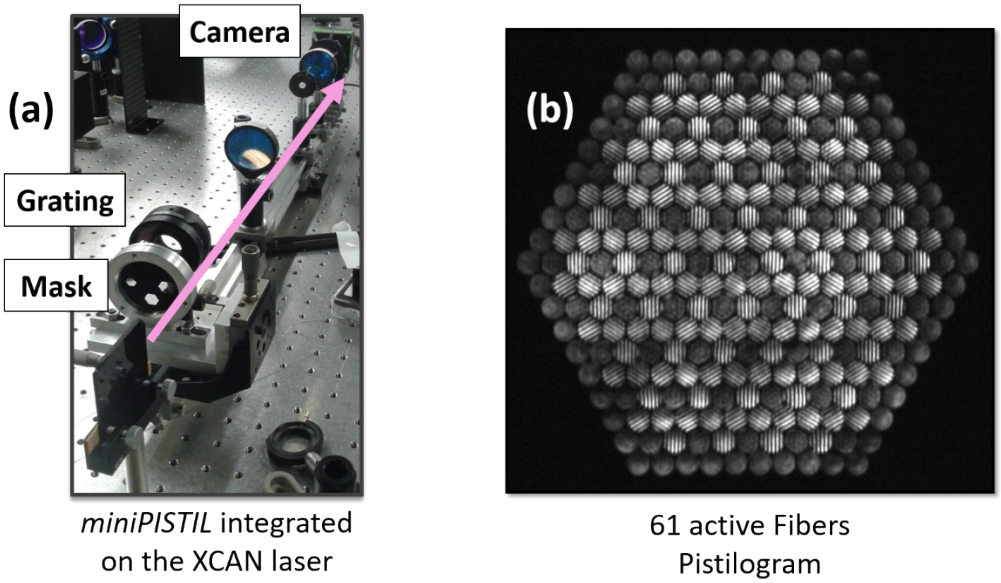

Figure 2: The miniPISTIL installation (a) and a related pistilogram (b).

3. Conditions of laser operation and measurement method

The purpose of our experiments is to study the phenomenology of open-loop phase noise in a stacked population of fiber lasers. To this end, the start-up procedure of the XCAN laser bench is reproduced to ensure that a thermal regulation of the laboratory is achieved [7]. The procedure lasts about 30 minutes, during which the PISTIL interferometer is also switched on, and a laser calibration is being done. Indeed, as the XCAN laser operates in the pulse regime,

a channel delays compensation is necessary to improve fringes contrast on the pistilograms. This is being made by remotely mechanically acting on the DPAM to correct the delay of all beams. Once it is done, there is no need to modify furthermore the state of the fiber lasers, which are therefore left in an open-loop operating state. We also took advantage of this moment to perform a measurement of the residual phase of the closed-loop and found an average value of $\lambda/50$ RMS, which corroborates the result of [7], enounced in section 2.

Temporal phase variation measurements are being recorded on the PISTIL interferometer computer and processed afterward from pistilograms to time series formats. For each experiment, the phase piston reference value is arbitrarily set to zero rad at t = 0 s to simplify the reading.

The measurements are recorded for 200 W and 760 W total average power while only 57 fiber amplifiers were operated, at a repetition rate of 423 kHz. Let us notice that this relatively low repetition rate means that the laser was operated in a non-linear/high average power regime for the 760 W experiment. On one hand, the non-linear regime means that the amount of energy per pulse increases consequently affecting the temporal pulse quality due to the apparition of self-phase modulation. The spectral phase is then affected by the peak power of the pulse itself, which often calls for the need to quantify the B-integral of the latter. For the case of the XCAN laser, this study has been conducted in detail in reference [16], and concluded that it was possible to operate each laser source while it accumulated a B-integral of 2.4 rad. In this paper, the same conditions apply. On the other hand, the high average power implies higher thermal load also responsible for phase distortions.

4. Experimental results and discussions

As an initial observation of the results, the open-loop phase time series reveal both similarities and clear differences when graphically displayed (figure 3). First, on most of our observations, the largest extensions of the channel phases seem to be reached for the external channel positions in the fiber array, regardless of the measurement scales. In Figure 3 are shown all the phase time series plotted altogether for a total average pupil power of 200 W, with a dotted cone that limits the area within which most of the phase excursions occur. For the rest of the paper, the fibers and their associated phase noises, as well as their computations, will be indexed according to the map displayed in the inset. To illustrate our purpose for single fiber behaviors, a focus on fiber 1 and 25 will be set as an example. Fiber 1 is chosen in a generic way because most channels have the same characteristics, while fiber 25 is one of some fibers with very different behavior.

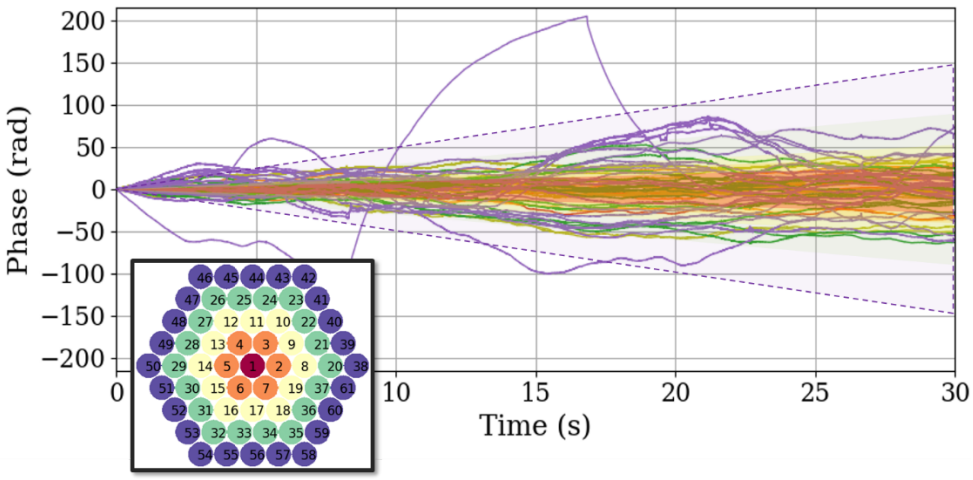

Figure 3: Multiple phase time series plots from the XCAN array (average pupil power of 200 W, repetition rate of 423 kHz). The dotted cone limits the area within which most of the phase excursions occur. This can be repeated for each ring of the hexagonal array (color matches). Very extended variations seem more likely for the channels at the edge of the fiber array (purple).

Let us now have a closer look at the evolution of the phase with the average power of the laser array. In the insets of Figure 4 and Figure 5 are displayed the phases of channels 1 and 25 respectively for the same timescale of 1 second, for two power levels registered at the repetition rate of 423 kHz (see section 3). Phase value axis is however varying in the plots. Different oscillation frequencies can be distinguished between the two channels. This suggests investigating about the spectral content of the datasets.

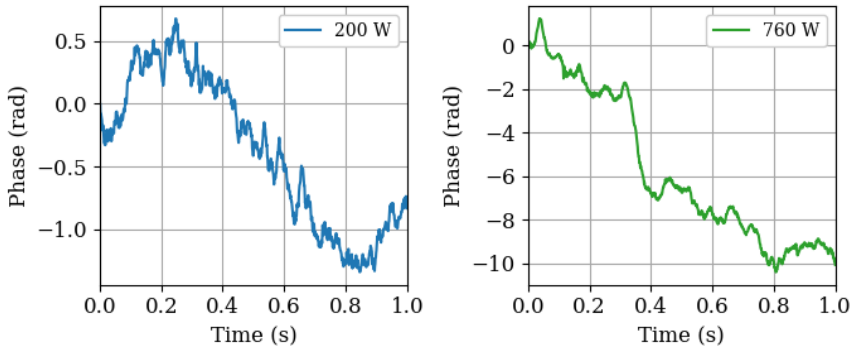

Figure 4: Phase time series for the Channel 1, for two different average power levels.

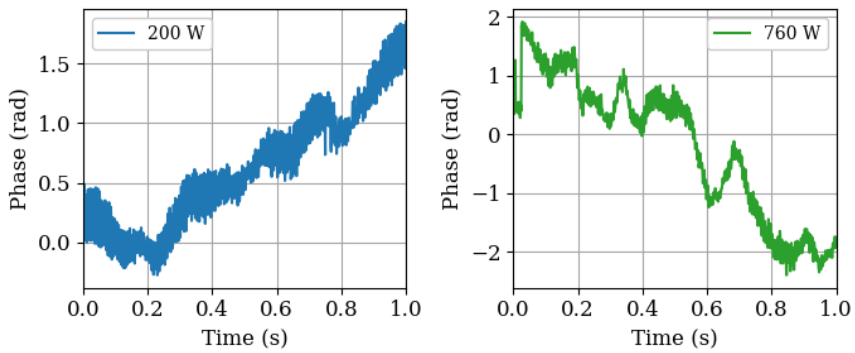

Figure 5: Phase time series for the Channel 25, for two different average power levels.

Power spectral densities (PSD) are then computed for all the time series (corrected from their time offsets and slopes to avoid 0-Hz blur). In the insets of Figure 6 and Figure 7 are displayed the phases of channels 1 and 25 respectively. The first distinction concerns characteristic frequencies also called spurs: very easily identifiable for PSD #25 (the most easily discernible being the 170 Hz one, that is why we choose it as an illustrative example), they are much less so for PSD #1: only a weak spur around 40 Hz is substantially discernible for the power level of 200 W. This observation is repeated for different channels, different power levels, and different characteristic frequencies.

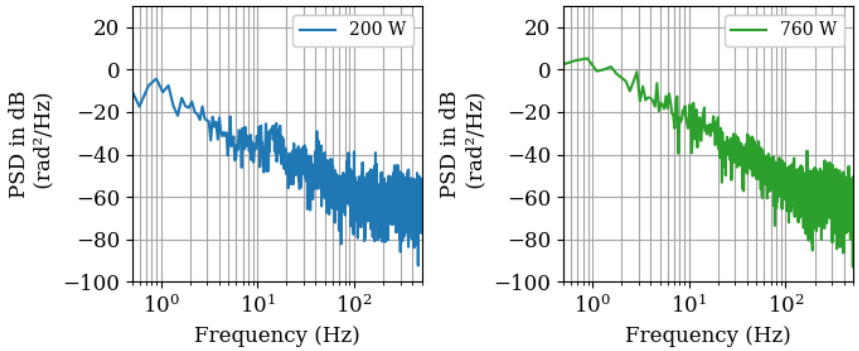

Figure 6: Power spectral densities for the channel 1, for two different average power levels.

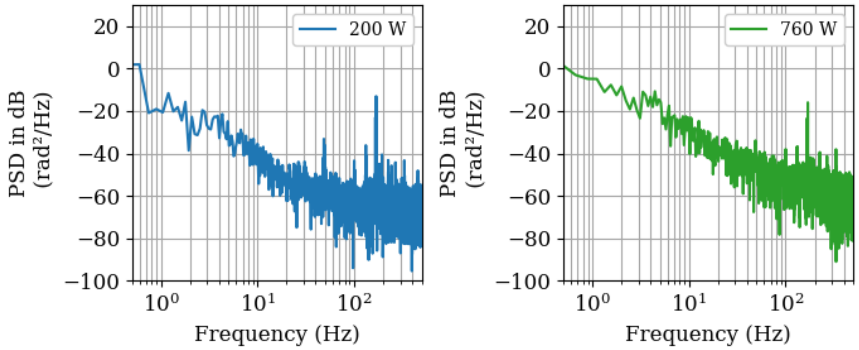

Figure 7: Power spectral densities for the channel 25, different average power levels. In contrast with the PSD of channel 1, spurs in between 100 to 400 Hz are here visible.

The spurs RMS contributions associated to the observed characteristics frequencies in the phase PSD of each channel can also be measured by computing the Integrated Phase Noise (IPN). This figure of merit is obtained for the n-th channel by taking the square root of a gradual PSD integration done backward (say, from $f_M = 500$ Hz down to 1 Hz):

$$IPN_n(f) = \sqrt{\int_{f_M}^{f} PSD_n(\nu)d\nu}\,. \quad (1)$$

It has been used in previous CBC-related work to derive the proportion of noise that can be contained within a certain spectral range of the signal or as a tool for open versus closed loop comparison [23-25]. Here, the IPN is computed around the 170 Hz spurs (from $f_M = 180$ Hz to $f = 160$ Hz) for each channel and the result is displayed into the 2D map of Figure 8. This representation allows determining quickly which channels present some features at 170 Hz, with their intensities (values of the integral) in rad and their spatial arrangements.

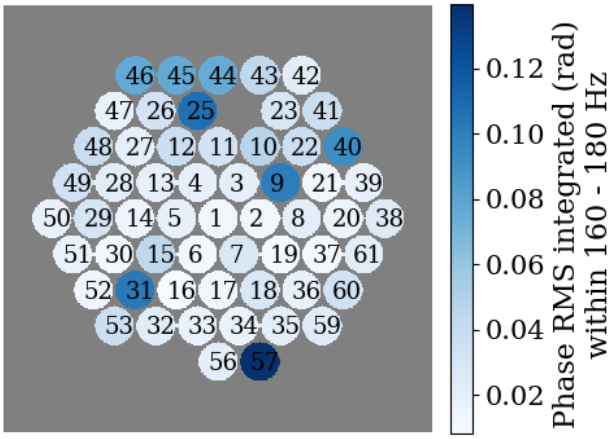

Figure 8: Phase RMS integrated within the (160-180) Hz spectral range by the integrated phase noise formulae, for an average power level of 200 W, and while only 57 active fibers were available during the experiment. Saturated blue tokens indicates strong spectral features near the 170 Hz peak.

The spectral analysis by the PSD or IPN criterion provides information on regular noise (with a feature such as the 170 Hz spur) or random noise (slope of PSD) compositions. According to the discussion of [26], these two aspects of the phase power spectrum are related to mechanical and thermal phenomena respectively. Taking note of the disparities between these two phenomena allows either the conceiver or the end-user of the fiber array, to carry out an easier diagnosis and maintenance of the channels. On the XCAN laser, the practical assembly of the laser channels, on plates that bring the amplified fibers to the laser head, means that the spatial (and thus mechanical) distribution of the fibers is susceptible to disturbances (see [27]). We can suppose that these are those small differences in the assembly, or in one of the electro-optical sub-system (such as the DPAM, pre-amplifiers), which make appear features such as the 170 Hz spur taken as example.

Yet, for the applications of these fiber laser populations, and in particular the design of a phase control loop, one must also be interested in the instantaneous behavior of the phase. For that, it is interesting to introduce a temporal criterion. So, to quantify the average absolute phase accumulation with time, which by the way allows calibrating the correction frequency of a control loop, the first phase Structure Function (SF) was calculated. Presented in the characterization of [28], it is defined for the n-th channel phase $\varphi_n(t)$ as follow:

$$SF_n(\tau) = \langle|\varphi_n(t) - \varphi_n(t+\tau)|\rangle. \quad (2)$$

This function evaluates the phase deviation after a certain time shift τ. The averaging is made over a 1 second window, yet no changes were observed if extended. Evolution of SF #1 and SF #25 are displayed within Figure 9 and Figure 10, respectively. The red dashed line symbolizes a phase accumulation limit for a closed loop (nowadays typically $\lambda/50$ RMS, therefore $2\pi/50 = 0.13$ rad RMS). Several observations can be made from this calculation.

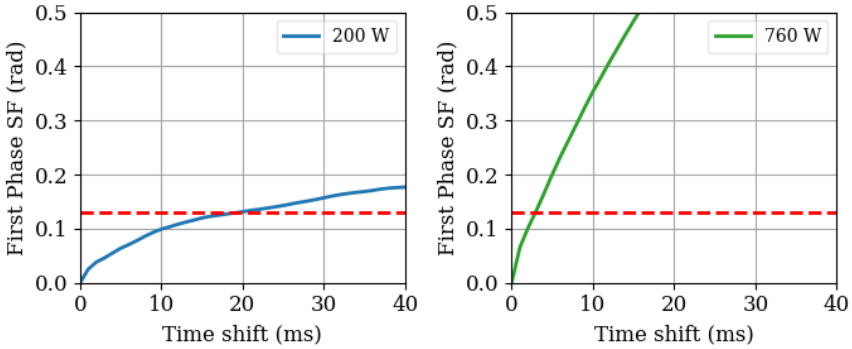

Figure 9: First phase structure function for the Channel 1, different average power levels, first 40 ms. The dashed red line is a $\lambda/50$ typical closed-loop indicator.

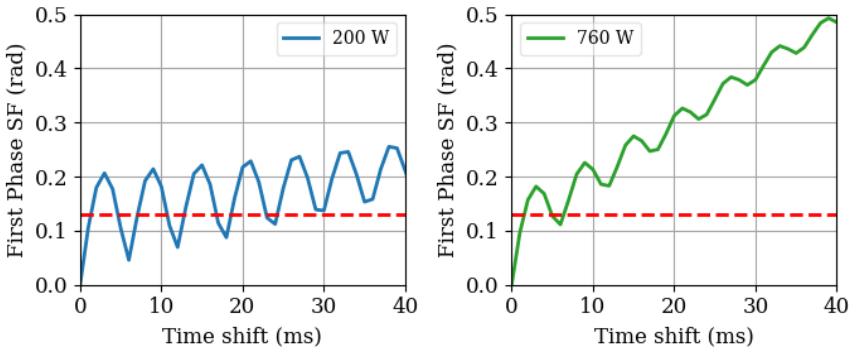

Figure 10: First phase structure function for the Channel 25, different average power levels, first 40 ms. The dashed red line is a $\lambda/50$ typical closed-loop indicator.

The distinction that has been made with the PSDs on the presence or not of characteristic frequencies (e.g. the 170 Hz one in Figure 7) is found here, and in a much accentuated way. Indeed, this frequency is retrieved in the absolute phase accumulation as responsible for the pseudo-periodic behavior of the SF #25 (root of the first lobe is ~ 5.9 ms, which corresponds to $\sim$ 170 Hz).

Here, to keep a phase accumulation limit under $\lambda/50$ RMS as example, one must choose closed-loop bandwidths for SF #1 in range from 50 Hz up to 100 Hz for 200 W power (and also at 460 W) and then 1 kHz for the 760 W high-power, non-linear regime. On the other hand, bandwidths for SF #25 look stretched to > 500 Hz minimal requirement because of the observed oscillatory noise. If this one would be filtered out, one can imagine that the smoothing of SF #25 curve will push forward in time the crossing point with the red dashed line, leading to bandwidths estimates close to those of the channel 1.

We finally measured the slopes of the PSD of our fiber laser test population and fitted it by a log-log regression. There were few variations in the slope depending on the channel index or the average power level: mean and standard deviation slope values are gathered in the Table 1

for four average power levels. However, no specific spatial distribution were highlighted neither in several similar average power measurements, nor a change in the latter. Typical PSD slope map is shown as example in Figure 11.

Although no remarkable change nor issue were spotted in our current results, we believe that this way of measuring the phases of the fibers as well as representing them will allow identifying very quickly a change on the fiber population behavior. Indeed, a significant change in the slope value (varying either with fiber index or average power level), will indicate that a disturbance phenomenon, has most likely occurred along the considered laser channel. The latter may lead to investigation of the potential sources of the change, whether in the thermal or acoustic/mechanical regime [25, 26].

Table 1: Mean slopes of the log-log regression and their standard deviations.

Average pupil power	20 W	200 W	460 W	760 W
Mean slope	-2.4	-2.6	-2.3	-2.5
Standard deviation	0.5	0.4	0.4	0.5

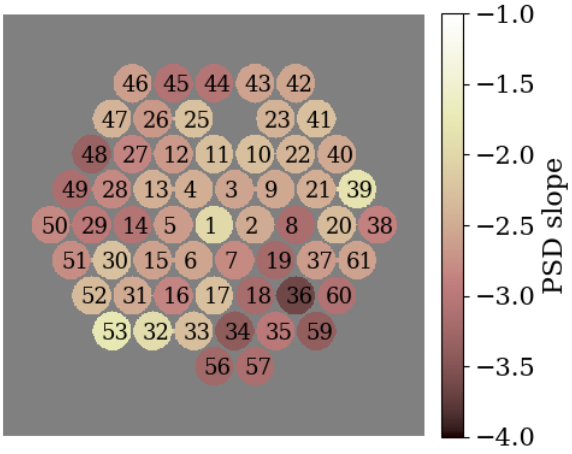

Figure 11: PSD slope map example for the average power level of 200 W, and the 57 active fibers of the array. On the opposite of the spur recurrences, here the distribution will show no spatial arrangement for either multiple measurements, or power level changes.

Similar to the search for spurs in PSD (Figure 8), this approach raises the interest of having a phase metrology mean for a laser array at any stage of design: stacking of fibers, open-loop and closed-loop operation.

5. Conclusion

In this paper, we present various open-loop phase noise diagnoses of the XCAN fiber laser array, enabled by the collective phase measurement allowed by a PISTIL interferometric sensor. We illustrate how a large set of fiber laser channels can be simultaneously analyzed to estimate their respective phase variations and associated PSDs. This study reveals that most of the setup of the fibers in practice always presents mechanical differences in positioning. No modal behavior of a channel grouping in the array has been observed.

Still, clear differences in spectral analysis reveal some channels here and there are more affected by features or spurs, such as a distinct mechanical vibration (e.g. the 170 Hz spur discussed in the paper), maybe originating from the practical positioning of the fibers on the laser front-end route. These differences are observable not only through the analysis of PSDs

but also through figures of merit from previous CBC studies, such as the phase Structure Function. They show here a renewed usefulness today for the characterization of a large number of open-loop fiber lasers.

Despite these local differences, the PSD law of the channel phase variation appears to be the same, with a mean slope of -2.4 regardless the average power of the fiber array. This slope value is close to the one of a random walk (-2), which seems to us to be a convenient way from now on to simulate phase noise in the laser channels for the pre-dimensioning of a fiber array, instead of using white noise. This is especially valuable in the thermo-mechanical regime (up to 0.1-1 kHz). It will also be handy to include local phenomena such as the observed spurs in this regime, as their sporadic nature over the array could make them potentially detrimental to a phasing loop taken from the CBC literature.

Finally, we believe that our experimental open loop phase measurements and our recommendation for future simulations will pave the way to optimize a servo loop algorithm for CBC, or even the way they are handled by standard technological components. Two perspectives emerge from our work. The first is to show that the PISTIL open-loop metrology is able to measure other fundamental parameters, such as the delays between ultrashort beams and the intensity map of the array. The second would be to include the PISTIL interferometer in a CBC phase control loop.

Funding

This work is supported by “Investissements d’Avenir” LabEx PALM (ANR-10-LABX-0039-PALM).

Disclosures

The authors declare no conflicts of interest.

Data availability

Data underlying the results presented in this paper are not publicly available at this time but may be obtained from the authors upon reasonable request.

References

1. E. Shekel, Y. Vidne, and B. Urbach, "16kW single mode CW laser with dynamic beam for material processing," Proc. SPIE **11260**, 1126021 (2020).
2. C Prieto, E. Vaamonde, D. Diego-Vallejo, J. Jimenez, B. Urbach, Y. Vidne, and E. Shekel "Dynamic laser beam shaping for laser aluminium welding in e-mobility applications," Proc. SPIE **11260**, 1126021 (2020).
3. D. C. Jones, A. J. Turner, A. M. Scott, S. M. Stone, R. G. Clark, C. Stace, and C. D. Stacey, "A multi-channel phase locked fibre bundle laser," Proc. SPIE **7580**, 75801V (2010).
4. G. A. Mourou, D. Hulin, and A. Galvanauskas, “The road to high peak power and high average power lasers: Coherent amplification network (can),” AIP Conference Proceedings **827**(1), 152-163 (2006)
5. Z. Liu, X. Jin, R. Su, P. Ma, P. Zhou, “Development status of high power fiber lasers and their coherent beam combination,” in Journal of Science China Information Sciences, Vol. **62** (4), 041301- (2019).
6. M. Müller, A. Klenke, A. Steinkopff, H. Stark, A. Tünnermann, and J. Limpert, "3.5 kW coherently combined ultrafast fiber laser," Opt. Lett. **43**, 6037-6040 (2018).
7. I. Fsaifes, L. Daniault, S. Bellanger, M. Veinhard, J. Bourderionnet, C. Larat, E. Lallier, E. Durand, A. Brignon, and J.-C. Chanteloup, "Coherent beam combining of 61 femtosecond fiber amplifiers," Opt. Express **28**, 20152-20161 (2020).
8. H. Chang, Q. Chang, J. Xi, T. Hou, R. Su, P. Ma, J. Wu, C. Li, M. Jiang, Y. Ma, and P. Zhou, "First experimental demonstration of coherent beam combining of more than 100 beams," Photon. Res. **8**, 1943-1948 (2020).
9. T. Weyrauch, M. Vorontsov, J. Mangano, V. Ovchinnikov, D. Bricker, E. Polnau, and A. Rostov, "Deep turbulence effects mitigation with coherent combining of 21 laser beams over 7 km," Opt. Lett. **41**, 840-843 (2016).
10. B. Rouzé, L. Lombard, H. Jacqmin, A. Liméry, A. Durécu, and P. Bourdon, "Coherent beam combination of seven 1.5 µm fiber amplifiers through up to 1 km atmospheric turbulence: near- and far-field experimental analysis," Appl. Opt. **60**, 8524-8533 (2021).

11. D. Kabeya, V. Kermène, M. Fabert, J. Benoist, J. Saucourt, A. Desfarges-Berthelemot, and A. Barthélémy, "Efficient phase-locking of 37 fiber amplifiers by phase-intensity mapping in an optimization loop," Opt. Express **25**, 13816-13821 (2017).
12. M. Antier, J. Bourderionnet, C. Larat, E. Lallier, E. Lenormand, J. Primot, and A. Brignon "kHz Closed Loop Interferometric Technique for Coherent Fiber Beam Combining," in IEEE JSTQE, vol. **20** (5), 182-187, (2014).
13. C. Geng, W. Luo, Y. Tan, H. Liu, J. Mu, and X. Li, "Experimental demonstration of using divergence cost-function in SPGD algorithm for coherent beam combining with tip/tilt control," Opt. Express **21**, 25045-25055 (2013).
14. S. J. Augst, T. Y. Fan, and A. Sanchez, "Coherent beam combining and phase noise measurements of ytterbium fiber amplifiers," Opt. Lett. **29**, 474-476 (2004).
15. M. Veinhard, S. Bellanger, L. Daniault, I. Fsaifes, J. Bourderionnet, C. Larat, E. Lallier, A. Brignon, and J.-C. Chanteloup, "Orbital angular momentum beams generation from 61 channels coherent beam combining femtosecond digital laser," Opt. Lett. **46**, 25-28 (2021).
16. A. Heilmann, J. Le Dortz, L. Daniault, I. Fsaifes, S. Bellanger, J. Bourderionnet, C. Larat, E. Lallier, M. Antier, E. Durand, C. Simon-Boisson, A. Brignon, and J.-C. Chanteloup, "Coherent beam combining of seven fiber chirped-pulse amplifiers using an interferometric phase measurement," Opt. Express **26**, 31542-31553 (2018).
17. M. Deprez, C. Bellanger, L. Lombard, B. Wattellier, and J. Primot, "Piston and tilt interferometry for segmented wavefront sensing," Opt. Lett. **41**, 1078-1081 (2016).
18. M. Deprez, B. Wattellier, C. Bellanger, L. Lombard, and J. Primot, "Phase measurement of a segmented wave front using PISton and TILt interferometry (PISTIL)," Opt. Express **26**, 5212-5224 (2018).
19. B. Rouze, J. Primot, P. Lanzoni, F. Zamkotsian, F. Tache, and C. Bellanger, "High-dynamic range segmented mirror metrology by two-wavelength PISTIL interferometry: demonstration and performance," Opt. Express **28**, 32415-32425 (2020).
20. B. Rouzé, J. Primot, F. Zamkotsian, P. Lanzoni, C. Bellanger, "PISTIL interferometry: a modular, plug-and-play metrology mean for diagnosis of coherently combined laser arrays," Proc. SPIE **11665**, 116651K (2021).
21. B. Rouzé, S. Bellanger, I. Fsaifes, C. Bellanger, M. Veinhard, J.-C. Chanteloup, and J. Primot, "PISTIL interferometry diagnosis on a 61 channels coherent beam combining digital laser," CLEO/Europe-EQEC 2021, (2021).
22. J. Le Dortz, A. Heilmann, M. Antier, J. Bourderionnet, C. Larat, I. Fsaifes, L. Daniault, S. Bellanger, C. Simon-Boisson, J.-C. Chanteloup, E. Lallier, and A. Brignon, "Highly scalable femtosecond coherent beam combining demonstrated with 19 fibers," Opt. Lett. **42**, 1887-1890 (2017).
23. S. J. Augst, J. K. Ranka, T. Y. Fan, and A. Sanchez, "Beam combining of ytterbium fiber amplifiers (Invited)," J. Opt. Soc. Am. B **24**, 1707-1715 (2007).
24. P. Zhou, X. Wang, Y. Ma, J. Leng, H. Ma, J. Wang, X. Xu, and Z. Liu, "Phase-locking of rapidly changing phase fluctuations in a strongly pumped fibre amplifier using a stochastic parallel gradient descent controller, " *Journal of Physics B: Atomic, Molecular and Optical Physics*, vol. **42**, nº 19, p. 19540 (2009).
25. L. Lombard, G. Canat, A. Durecu, P. Bourdon, "Coherent beam combining performance in harsh environment," Proc. SPIE **8961**, 896107 (2014).
26. L. Lombard, C. Bellanger, G. Canat, L. Mugnier, F. Cassaing, V. Michau, P. Bourdon, and J. Primot "Collective synchronization and phase locking of fs fiber amplifiers: Requirements and potential solutions," *Eur. Phys. J. Spec. Top.* **224,** 2557–2566 (2015).
27. J.-C. Chanteloup, S. Bellanger, L. Daniault, I. Fsaifes, M. Veinhard, J. Bourderionnet, C. Larat, E. Lallier, and A. Brignon, "61 channels coherent beam combining femtosecond digital laser," Proc. SPIE **11665**, 116651H (2021).
28. D. C. Jones, C. D. Stacey, and A. M. Scott, "Phase stabilization of a large-mode-area ytterbium-doped fiber amplifier," Opt. Lett. **32**, 466-468 (2007).